PREDICTIONS OF CRITICAL HEAT FLUX USING THE ASSERT-PV SUBCHANNEL CODE FOR A CANFLEX VARIANT BUNDLE

EBRU NIHAN ONDER, LAURENCE KIM-HUNG LEUNG* and YANFEI RAO
Atomic Energy of Canada Limited, Thermalhydraulics Branch, Chalk River Laboratories
Chalk River, Ontario Canada K0J 1J0.
*Corresponding author. E-mail : leungl@aecl.ca

Invited March 21, 2008
Received October 30, 2008

The ASSERT-PV subchannel code developed by AECL has been applied as a design-assist tool to the advanced CANDU®[1] reactor fuel bundle. Based primarily on the CANFLEX®[2] fuel bundle, several geometry changes (such as element sizes and pitch-circle diameters of various element rings) were examined to optimize the dryout power and pressure-drop performances of the new fuel bundle. An experiment was performed to obtain dryout power measurements for verification of the ASSERT-PV code predictions. It was carried out using an electrically heated, Refrigerant-134a cooled, fuel bundle string simulator. The axial power profile of the simulator was uniform, while the radial power profile of the element rings was varied simulating profiles in bundles with various fuel compositions and burn-ups. Dryout power measurements are predicted closely using the ASSERT-PV code, particularly at low flows and low pressures, but are overpredicted at high flows and high pressures. The majority of data shows that dryout powers are underpredicted at low inlet-fluid temperatures but overpredicted at high inlet-fluid temperatures.

KEYWORDS : CHF, Bundle, Subchannel Code, ASSERT-PV, CANDU Reactor

1. INTRODUCTION

Prediction of critical heat flux (CHF) in rod bundles is important in establishing the thermalhydraulic performance. CHF is one of the licensing parameters for safe reactor operation. Correlations have been derived using full-scale bundle test data for predicting CHF in existing fuel bundle designs. A subchannel code is often used as a design-assist tool for quantifying the thermalhydraulics performance of new fuel bundles. It has the flexibility to examine the impact of geometry and flow condition variations on thermalhydraulic characteristics, and hence is the ideal tool for design optimization. Testing is then performed to provide confirmatory data for the new design.

AECL has developed the ASSERT-PV code for examining subchannel flow and enthalpy behaviours in CANDU fuel bundles [1-2]. The code has been applied to support the new design of CANDU fuel bundle [3]. Based primarily on the CANFLEX fuel bundle, the impact of geometry and pitch-circle-diameter changes on dryout power has been examined. The optimized geometry consists of a large centre element and 42 elements of the same size distributed in three rings. Pitch-circle diameters of these element rings in the new fuel bundle design (referred to as CANFLEX Variant bundle) differ slightly from those in the CANFLEX fuel bundle.

An experiment was performed to obtain dryout power measurements for verification of the ASSERT-PV prediction capability to account for the geometry variation. A CANFLEX bundle simulator was modified to include a large centre element and 42 elements of the same size. Dryout power measurements obtained from the experiment were used to assess the predictions of the ASSERT-PV code. Objectives of this paper are to describe the experimental set-up, present the dryout power measurements, and compare experimental data and ASSERT-PV predictions of dryout power and CHF.

[1] CANDU® (CANada Deuterium Uranium) is a registered trademark of Atomic Energy of Canada Limited (AECL).
[2] CANFLEX® - CANDU Flexible, a registered trademark of AECL and KAERI (Korea Atomic Energy Research Institutes).

2. EXPERIMENTS

Dryout-power experiments were performed with the bundle simulator installed inside the vertical test station

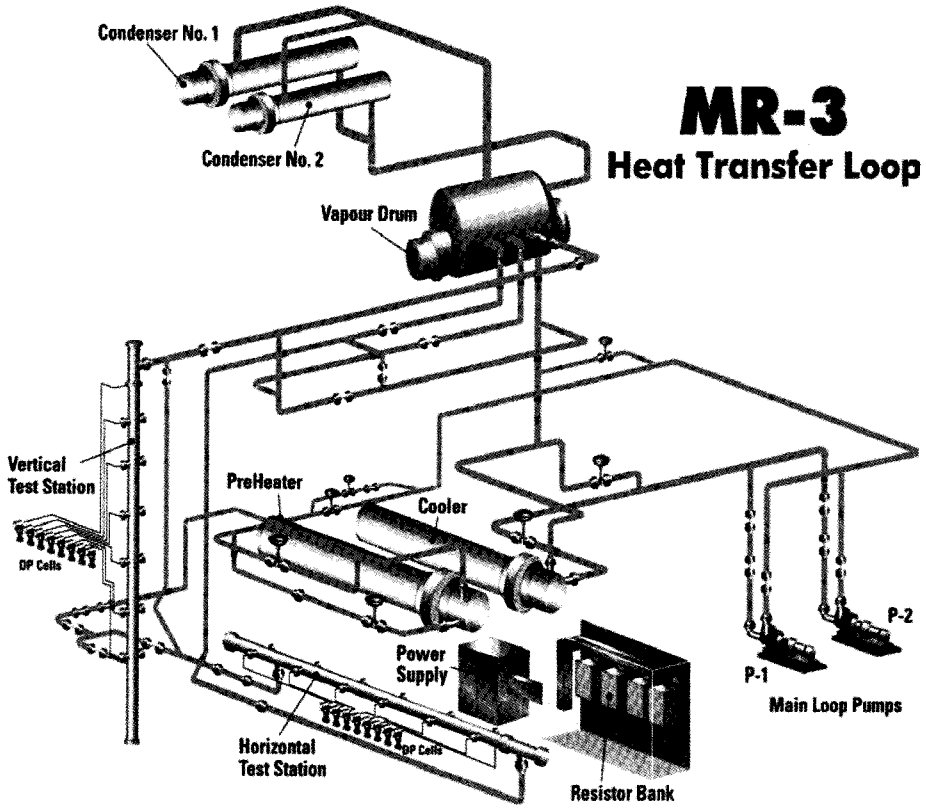

Fig. 1. MR-3 Freon Loop at Chalk River Laboratories

of the MR-3 Freon loop (see Figure 1) at Chalk River Laboratories (CRL). Refrigerant R-134a was used as the working fluid, and subcooled fluid was supplied to the test station using two recirculating pumps. These pumps are capable of recirculating up to 38 kg/s of fluid at a maximum test station outlet pressure of 2.7 MPa. The coolant temperature at the inlet of the test station was controlled with a pre-heater located downstream of these pumps. Coolant entering the test station was heated along the simulator and discharged into a vapor drum where the vapor condensed. The condensate returned to the circulating pumps.

2.1 Test Station

The vertical test station consisted of an 8-m long, 15-cm Schedule-40 carbon-steel pipe, acting as the pressure boundary for the flow tube and string simulator. Figure 2 illustrates the vertical test station and pressure-tap locations. A composite epoxy-fibreglass flow tube with an inside diameter of 103.45 mm was inserted inside the test station to house the bundle simulator. The flow tube acted also as an electrical insulator between the directly heated bundle simulator and carbon-steel test station. The coolant entered the test station near the upstream end (upstream of the bundle L in Figure 2), where it circulated around the external side of the flow tube and entered the flow tube at the upstream end. This eliminated the cross-flow at the entry point and reduced the entrance effect. The coolant discharged from the flow tube at the downstream end (downstream of bundle A) of the test station. It circulated around the external side of the flow tube and left the test station near the downstream end.

2.2 Fuel Bundle Simulator

The 5.94-m long electrically heated bundle simulator was constructed to simulate as closely as possible the external shape and dimension of a string of 12-aligned CANFLEX bundles with end-plates, bearing pads, CHF enhancement buttons, and spacers. Each bundle segment consisted of 487.6-mm long Inconel-718 tubes jointed by nickel-plated brackets at the spool pieces, forming a ring. The length in the heated section was reduced from brazing of the tube to the spool piece. Brackets at neighbouring rings were joined with fibreglass webs, which act as an insulator. These brackets simulated circular webs, and fibreglass webs simulated cross webs of an endplate in the CANFLEX bundle. The simulator had the overall configuration of a CANFLEX bundle, except that the centre-element diameter was increased to 18 mm and the diameter of inner-ring elements was reduced to 11.5 mm (see Figure 3). Pitch-circle diameters were kept the same

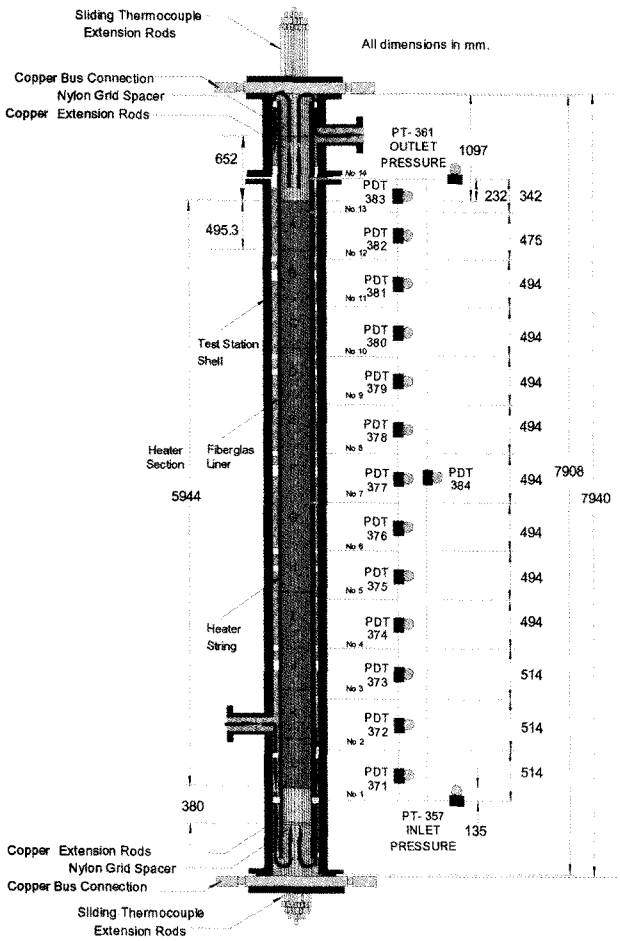

Fig. 2. Vertical Test Station with Pressure Tap Locations

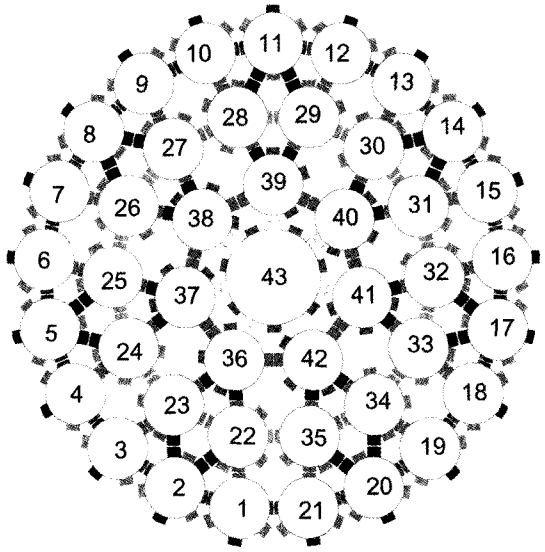

Fig. 3. Cross-Sectional Geometry of Bundle Simulator and Element Identification

as those in the CANFLEX bundle.

Sizes and configurations of most appendages were maintained the same as those in the CANFLEX bundle. Element rings of the bundle were electrically insulated from each other using spot-welded insulated spacer pads between adjacent rings and fibreglass webs between adjacent ring segments in the endplates. Spacers on the centre element and inner-ring elements were adjusted to fit gaps between neighbouring elements. Bearing pads were spot welded to the Inconel tubes in the outer ring. The simulator was kept eccentric inside the flow tube using stainless-steel springs simulating the gravity effect on the bundle in a horizontal channel. These springs were welded on five bearing pads at the simulated top position of the bundle. The calculated eccentricity[3] was 0.39 mm.

The test section was heated with a DC power supply having an electrical capacity of 1.7 MW at a maximum 145 V and 12 kA. A variable resistor bank connected in series to the power supply was used to vary the radial power profile. The resistor bank consisted of a set of adjustable resistors, each of which was connected in series to a current shunt and to the appropriate bundle ring. This set of resistors included two Inconel tubes for the inner-ring elements and the centre element, and two stainless steel pipes for the intermediate and outer ring elements. These tubes and pipes were connected at one end to the common power-supply bus through four current shunts. Moveable power clamps were connected to each ring in the test section via copper extension rods. These power clamps were adjusted to provide a pre-selected in-series resistance to each of the bundle rings. Measurements of voltage drop across each bundle ring and the current through each ring were used for the calculation of the power generated by each bundle ring.

The tube wall thickness was held constant over the length of the bundle string providing the uniform axial power distribution; however, it was varied among the ring element rings to provide non-uniform Radial Power Profiles (RPP). Four different radial power profiles were tested, simulating the fresh natural uranium (NU) fuel, 2% slightly enriched uranium (SEU) fuel at fresh and mid-burnups, and fresh graded SEU fuel (i.e., 2.1% SEU in the inner and outer rings, and 3.6% low enriched uranium (LEU) in the intermediate ring). Table 1 lists radial-power profiles (normalized to the outer-ring element power) and corresponding radial heat-flux distributions (RFD) (normalized to the average bundle heat flux) covered in the current experiment. Figure 4 demonstrates the RFD covered in the CHF tests.

[3] Distance between the bundle and the flow tube centre lines

Table 1. Radial Power and Heat-Flux Profiles Covered in the Experiment

Bundle	RPP (normalized to outer-ring element power)	RFD (normalized to average heat flux)
	Centre/Inner/Intermediate/Outer	
Equivalent NU fuel	0.600 / 0.869 / 0.824 / 1.000	0.426 / 0.965 / 0.915 / 1.111
Mid-Burnup 2% SEU fuel	0.447 / 0.559/ 0.773 / 1.000	0.344 / 0.673 / 0.931 / 1.204
Fresh 2% SEU fuel	0.222 / 0.481 / 0.667 / 1.000	0.182 / 0.618 /0.856 / 1.284
Fresh Graded SEU fuel	0.438 / 0.452 / 0.954/ 1.000	0.321 / 0.519 / 1.085 / 1.148

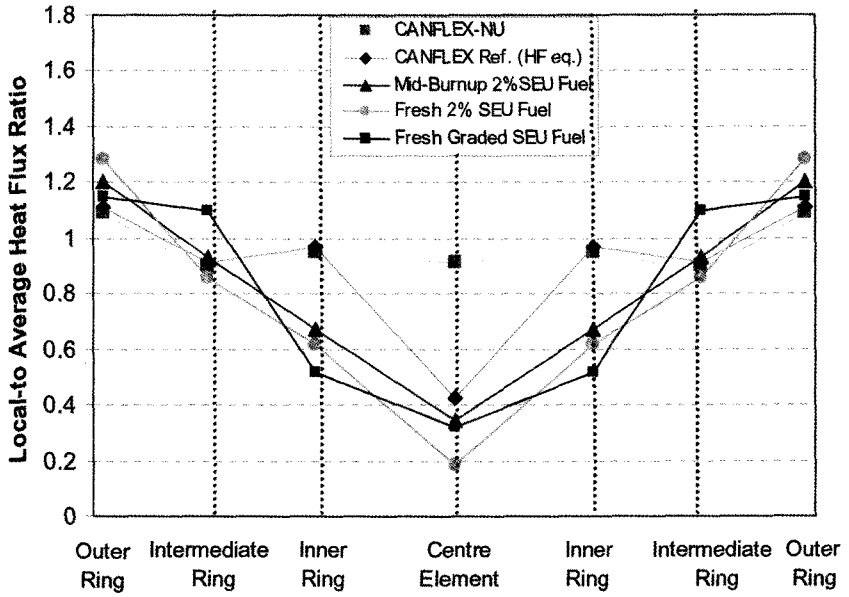

Fig. 4. Radial Heat Flux Distribution Corresponding to the Radial Power Profiles Covered in CHF Tests

2.3 Instrumentation and Data Acquisition System

Temperatures at the inlet and outlet of the test station were measured using calibrated resistor temperature devices (RTD). Pressures were measured at the inlet and outlet using calibrated pressure transmitters, and pressure drops along the test station were measured at the selected location (shown in Figure 2) with calibrated differential pressure transmitters. Calibrated two in-series flow meters were used for measurements of the mass flow rate in the test station.

For critical heat flux tests, 172 test-section-internal sliding thermocouples were installed in "A", "B", and "C" bundles (see Figure 2), and were primarily used as dryout indicators. Except the centre element in bundle "A", all elements in this bundle were equipped with two thermocouples at 180° circumferential locations in the same thermocouple carrier for back-up temperature measurements. Initial dryout was not anticipated to occur at the centre element. Moreover, for the current CHF tests, only the thermocouples in bundle "A" were monitored, as dryout occurs in the most downstream bundle with a uniform Axial Flux Distribution (AFD).

The data acquisition system (DAS) consisted of a network system of computers; each computer was multi-functional in providing data displays and trending, data storage and data archiving. The computing system monitored 360 analog inputs and provided full display, storage and printout capability for the test section and the MR-3 loop instrumentation. Data scanning and storage rates for the steady-state CHF tests were 0.2 scans per second (1 scan every 5 s) and 12 scans were taken for each data point. When automatic detection of dryout was implemented, the scan rate was set at 1 scan per second.

2.4 CHF Tests

At a given flow condition (i.e. outlet pressure, inlet temperature and flow rate), the power was increased in steps till the dryout was reached. The dryout was detected

by rotating the thermocouples within elements to identify a temperature spike by about 2 °C in the thermocouple trace, or to measure a significant temperature rise. Once the CHF was detected, the power was reduced to a level where the full rewetting of the bundle was ensured. The power was again increased to approach dryout. At dryout, all the signals monitored by the DAS were recorded by fixed-rate sampling and the data was stored on computer disc. Following the recording of the initial dryout conditions, the test section power was increased in small steps to observe and record dryout pattern as dryout spread radially across the bundle. At each subsequent dryout indication, the data was recorded by fixed rate sampling and stored on the computer disc. This procedure was followed to confirm initial dryout and to provide the evidence of dryout on additional rings in the bundle. At a given set of flow conditions, only an initial dryout indication was required. Upon completion of the subsequent dryout tests, power was reduced and another set of flow conditions was established for the next run.

The CHF experiment was carried out at the pressures of 1.84 MPa and 2.11 MPa (water equivalent values from 11.0 to 12.5 MPa), and covered the mass flow rates from 12.1 to 18.6 kg/s (water equivalent values from 17.0 to 26.0 kg/s), and inlet-fluid temperatures from 42.2 to 59.0 °C (water equivalent values from 260 to 300 °C). Water-equivalent values were established using fluid-to-fluid modelling [4].

3. ASSERT-PV CODE AND SIMULATIONS

ASSERT-PV has been developed at AECL to meet the specific requirements for the subchannel thermalhydraulic analysis of two-phase flows in the horizontally oriented CANDU fuel bundles. It provides detailed flow and phase distributions in subchannels of a fuel bundle to evaluate CHF, post-dryout heat transfer, and fuel-sheath temperature. It is the ideal computational tool for assessing the sensitivity of dryout power on changes in bundle geometry, such as changes in element diameter and pitch circle diameters.

The current release version of ASSERT-PV is ASSERT-PV V3R1 [2], which is used to predict dryout power in the present analysis. ASSERT-PV [2] is based on ASSERT-IV [1], which in turn was originated from the COBRA-IV computer program. The two-phase flow model used in ASSERT-PV is based on an advanced drift-flux model: a five-equation model that can consider thermal non-equilibrium and the relative velocity of the liquid and vapour phases. Thermal non-equilibrium is dealt with by two-fluid energy equations for the liquid and vapour. Relative velocity is obtained from semi-empirical correlations. While retaining the major features in ASSERT-IV, ASSERT-PV employs the more comprehensive and robust numerical solution based on the Pressure-Velocity numerical method to enhance the modelling capability under relatively low flows, among other ASSERT-PV improvements. The most up-to-date subchannel flow and enthalpy distribution models in ASSERT-PV are described in [5] including the single- and two-phase inter-subchannel turbulent mixing, void drift and diffusion, buoyancy drift, and the effect of bundle appendages.

Subchannel CHF prediction is also important in predicting channel dryout power. Dryout is considered to occur when the local heat flux in any one subchannel reaches the predicted CHF value at local subchannel-flow conditions. The corresponding channel power is referred to as the dryout power. ASSERT-PV V3R1 applies the LW-T-1996 CHF look-up table and its associated correction factors for diameter, gap size and flow orientation effects [7], in predicting the CHF value.

Changes in centre element and inner ring element diameters and pitch-circle diameters of various element rings have a significant impact on bundle CHF characteristics. These changes and the RFD were implemented into the existing ASSERT-PV model for the CANFLEX bundle. A set of ASSERT-model options, previously applied in the validation exercise of ASSERT-PV [2] against Stern Laboratories CANFLEX water CHF tests [6] has been used in this analysis with slight modifications. This set of model options was established from comparisons of code predictions against 37-element and CANFLEX bundle data. Slight modifications on some model options, such as the inter-subchannel mixing model coefficients, have been introduced based on a sensitivity study carried out during the validation exercise. They have also been examined and used in the analysis performed to optimize the bundle geometry for the CANFLEX Variant bundle [3].

Figure 5 illustrates the subchannel set up and identification numbers in the ASSERT-PV simulation of the CANFLEX bundle. The same subchannel set-up and identification numbers are used for the current bundle of interest.

4. ASSESSMENT OF ASSERT-PV

Dryout power measurements and corresponding CHF values were analyzed and shown to follow consistent trends with inlet-fluid temperature, mass flow rate, pressure, and dryout quality. These experimental values have been applied to assess the ASSERT-PV code for various radial power profiles at the tested range of flow conditions.

4.1 Dryout Power Prediction

The test results show that the initial dryout always took place on the outer-ring element at the bottom of the flow tube facing an inner subchannel. ASSERT-PV predicted the occurrence of the initial dryout in subchannel 36 either on Element 34 or on Element 35 (see Figure 5).

Figure 6 illustrates dryout power variations with inlet temperature and mass flow rate for the equivalent NU fuel profile at the outlet pressure of 1.84 MPa. As expected,

both experimental and predicted dryout powers decrease with increasing inlet temperature, and increase with increasing mass flow rate. Predictions of the ASSERT-PV code agree closely with measurements at inlet-fluid temperatures of about 49 °C. However, the predicted dryout power is slightly lower than the experimental value at low inlet-fluid temperature but higher at high inlet-fluid temperature. Similar trends were observed for other profiles.

Table 2 lists the prediction accuracy of ASSERT-PV for dryout power. Overall, ASSERT-PV predictions agree closely with experimental data. Except for the equivalent NU fuel profile, the agreement is better at the pressure of 2.11 MPa than 1.84 MPa. In general, it is observed that ASSERT-PV has a tendency to underpredict dryout powers for steep radial power profile (e.g., mid-burnup 2% SEU fuel) compared to those of relatively flat profiles (e.g., equivalent NU fuel profile).

The ASSERT-PV prediction capability of CHF is assessed against the experimental values with respect to local critical conditions (cross-sectional average values of pressure, mass flux and dryout quality). The outlet pressure corresponds closely to the dryout pressure since dryout occurs at the downstream end of the bundle with a uniform axial power profile. The cross sectional average mass flux in $kg \cdot m^{-2} \cdot s^{-1}$ is calculated with

$$G = \frac{W}{A_{flow}} \tag{1}$$

where W is the mass flow rate in $kg \cdot s^{-1}$, and A_{flow} is the flow area in m^2. The dryout quality, x_{DO}, (dimensionless) is expressed as

$$x_{DO} = \left[\frac{Dryout\ Power}{W} + \left(h_{in} - h_f \right) \right] \frac{1}{h_{fg}} \tag{2}$$

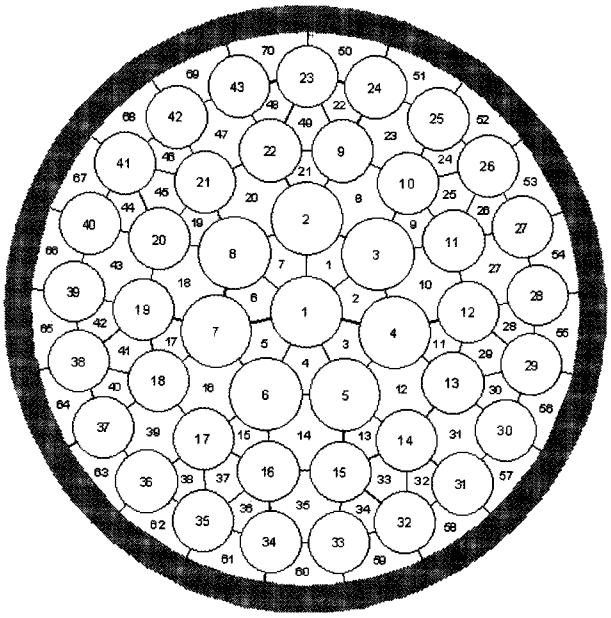

Fig. 5. Subchannel Set-up and Identification for the CANFLEX Bundle

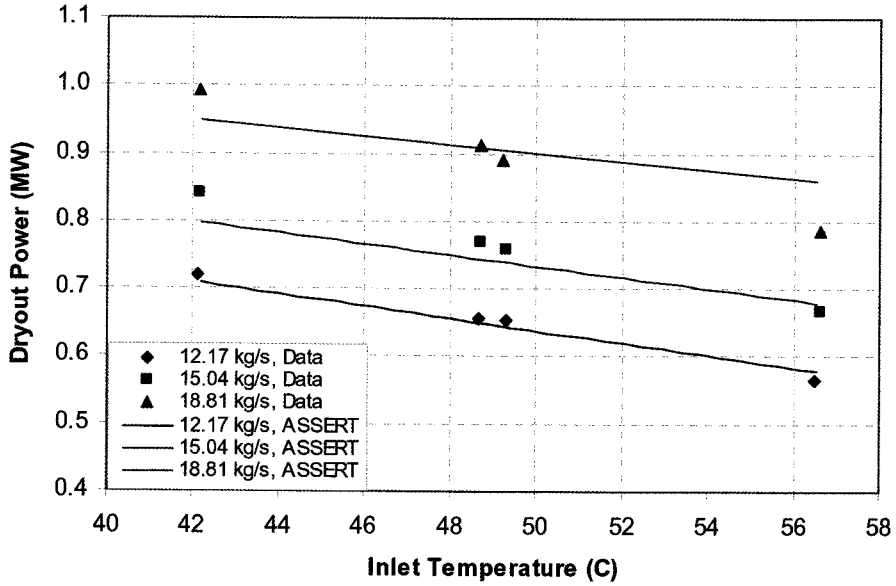

Fig. 6. Variation of Dryout Power for Equivalent NU Fuel Profile at the Pressure of 1.84 MPa

Table 2. Prediction Accuracy of ASSERT-PV on Dryout Power

Profile	OVERALL		1.84 MPa		2.11 MPa	
	Average Error[1] (%)	Standard Deviation[2] (%)	Average Error (%)	Standard Deviation (%)	Average Error (%)	Standard Deviation (%)
Equivalent NU fuel	1.1	3.8	-0.3	3.8	2.4	3.5
Mid-Burnup 2% SEU fuel	-0.6	3.6	-1.7	3.9	0.5	3.1
Fresh 2% SEU fuel	-1.4	4.0	-2.6	4.7	-0.2	2.8
Fresh Graded SEU fuel	-0.9	3.3	-1.9	3.6	0.1	2.8

[1] $Average\ Error = \overline{Error} = \frac{1}{n}\sum_{1}^{n}(Error)_i$;

where the prediction error is defined as $Error = \frac{\Pr edicted\ Value}{Experimental\ Value} - 1$

[2] $S\tan dard\ Deviation = \sqrt{\frac{1}{n-1}\sum_{i=1}^{n}\left(Error - \overline{Error}\right)_i^2}$

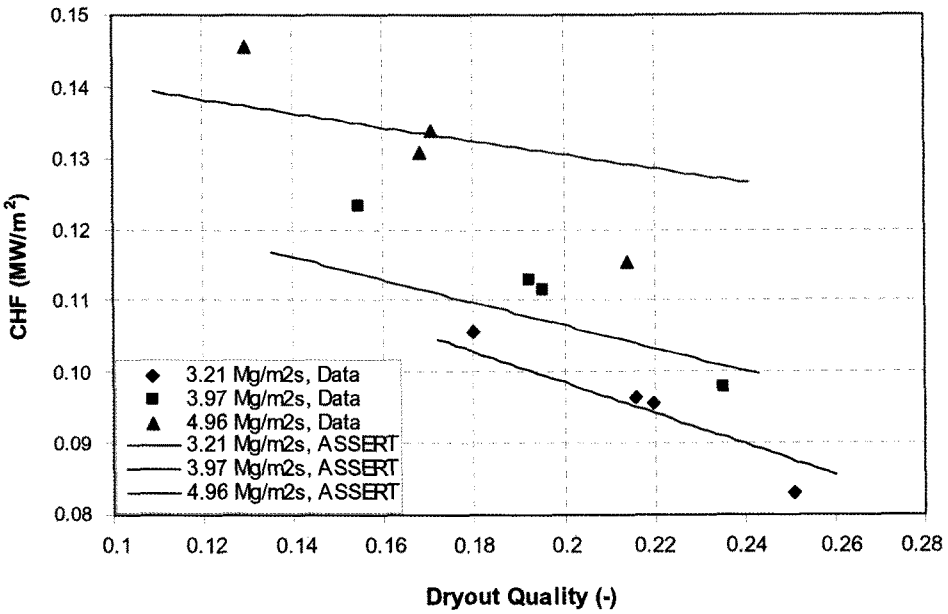

Fig. 7. Effect of Flow Conditions on CHF for the Equivalent NU Fuel Profile at the Pressure of 1.84 MPa

where Dryout Power is in Watts, h_{in} and h_f are the inlet and saturated liquid enthalpies, respectively, in $J \cdot kg^{-1}$, and h_{fg} is the latent heat of vaporization in $J \cdot kg^{-1}$. ASSERT-PV calculates local CHF in $W \cdot m^{-2}$ as

$$CHF = \frac{Dryout\ Power}{A_{heat}}(AFD)\frac{q_i}{q_{avg}} \tag{3}$$

where A_{heat} is the total heated area in m^2, AFD is the axial heat flux distribution, q_i is the local heat flux encountered within ring i, and q_{avr} is the average heat flux over the cross section of the bundle. As AFD is uniform, and CANDU safety analyses employed the 1-dimensional approach applying the cross-sectional average flow conditions and parameters, the CHF is calculated from

$$CHF = \frac{Dryout\ Power}{A_{heat}} \tag{4}$$

Figure 7 shows variations of CHF with dryout quality

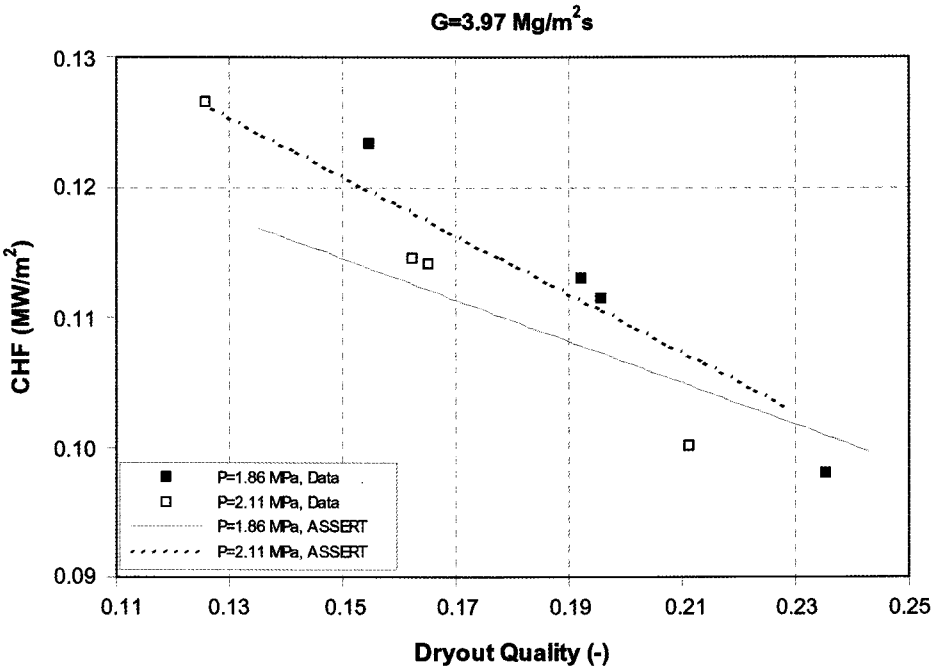

Fig. 8. Effect of Pressure on CHF for the Equivalent NU Fuel Profile at the Mass Flux of 3.97 $M \cdot m^{-2} \cdot s^{-1}$

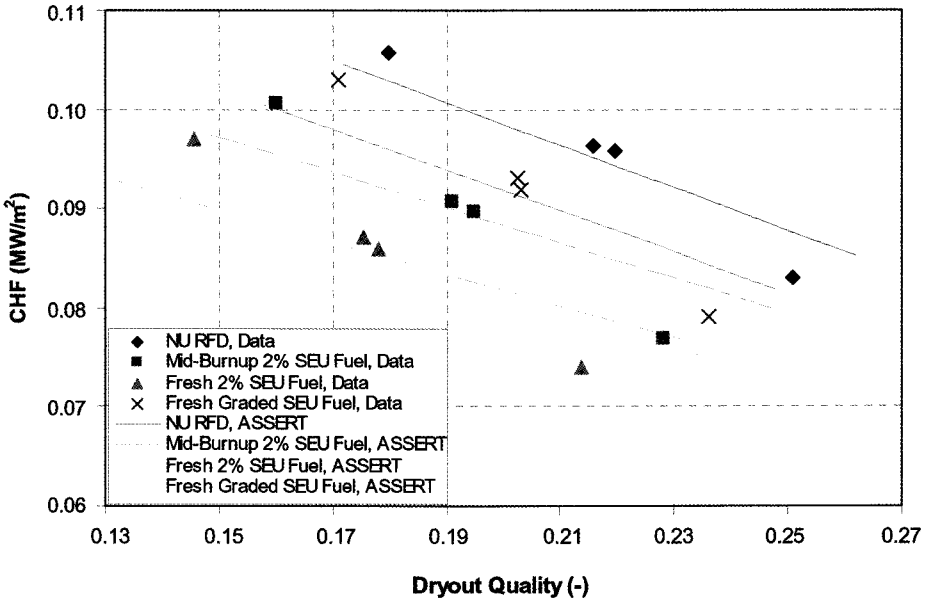

Fig. 9. Comparison of CHF for Different Radial Power Profiles at Pressure of 1.84 MPa and Mass Flux of 3.21 $Mg \cdot m^{-2} \cdot s^{-1}$

and mass flux for the equivalent NU fuel profile at the pressure of 1.84 MPa. The pressure effect on CHF at the mass flux of 3.97 $Mg \cdot m^{-2} \cdot s^{-1}$ is demonstrated in Figure 8. As expected, CHF decreases with increasing dryout quality and increasing pressure, and increases with increasing mass flux. The ASSERT-PV predicted CHF values lie generally within the range of the experimental CHF values. However, the experimental CHF trend is steeper than the predicted trend with dryout quality. On the other hand, predicted and experimental trends follow rather closely

with varying mass flux, as shown in Figure 7. In general, the experimental CHF values are underpredicted using the ASSERT-PV code at low qualities but are overpredicted at high qualities and at high pressure. Differences between experimental values and predictions are probably attributed to the applied modeling options, which were validated for CANFLEX bundle.

4.2 Effect of Radial Power Profile

Figure 9 shows experimental CHF values for various radial power profiles. The highest CHF value has been observed for the equivalent NU fuel profile, and the lowest value for the fresh 2% SEU fuel profile. CHF values for the graded SEU fuel profile are higher than those for the fresh and mid-burnup 2% SEU fuel profiles. ASSERT-PV predictions follow the same trend but with different slopes. Similar behavior has been observed at the outlet pressure of 2.11 MPa, and at other mass fluxes.

The overall impact of radial power profile is established from the CHF ratio between other fuel profiles and the NU fuel profile, i.e.,

$$(CHF\ Ratio)_{RFD} = \frac{CHF_{RFD}}{CHF_{NU}} \tag{5}$$

where CHF_{RFD} and CHF_{NU} are CHF values for the profile of interest and the NU fuel profile, respectively. To facilitate the comparison at the same local critical conditions, two correlations have been derived to represent CHF values (one for the experimental values and the other for ASSERT-PV predictions) for the NU fuel profile. The form of the correlation is the same, and is expressed as

$$CHF_{NU} = a_1 P^{b_1} G^{c_1} + d_1 P^{e_1} G^{f_1} x_{cr} \tag{6}$$

where a_1 to f_1 are the coefficients for the NU fuel profile representing the experimental and ASSERT-PV predicted CHF values. Table 3 lists the coefficients "a_1" to "f_1" for the NU RFD representing the experimental and ASSERT-PV predicted CHF values

Figure 10 compares predicted and experimental CHF ratios for various profiles (with the NU fuel profile as the reference). Overall, predicted CHF ratios using ASSERT-PV agree closely with experimental ratios. Table 4 summarizes average predicted and experimental CHF ratios for the three SEU fuel profiles. The predicted and experimental average CHF ratios are very similar; however

Table 3. Coefficients of Correlations for Experimental and ASSERT Predicted CHF Values

Derived For	Coefficients						CC[1]	CD[2]	SE[3]
	a_1	b_1	c_1	d_1	e_1	f_1	R	R^2	S_{yx}
Experiment	0.0952	-0.1855	0.5136	-0.1236	0.1752	0.5968	0.9979	0.9958	0.0013
ASSERT	0.0270	1.2833	0.5808	-0.0056	5.0889	-0.0920	0.9893	0.9788	0.0032

[1] Correlation Coefficient (R) is given by $R = \frac{\sum_{i=1}^{N}(x_i - \hat{x})(y_i - \hat{y})}{\sqrt{\sum_{i=1}^{N}(x_i - \hat{x})^2 \sum_{i=1}^{N}(y_i - \hat{y})^2}}$,

where xi is the independent variant, and $\hat{x}$ is the mean of the independent variants.

[2] Coefficient of Determination = R^2

[3] Standard Error of the Estimate is given by $S_{yx} = \sqrt{\frac{\sum_{i=1}^{N}(y_i - \hat{y})^2}{\nu}}$

where ν is the degrees of freedom of the fit, expressed as $\nu=N-(m+1)$, y_i is the dependant variable, $\hat{y}$ is the mean of the dependant variables within the set, N is the number of dependant variables, and m is the number of orders in the polynomial.

Table 4. CHF Ratios Based on Experimental Values and ASSERT-PV Predictions

Profile	Experiment		ASSERT-PV	
	CHF Ratio	Standard Deviation (%)	CHF Ratio	Standard Deviation (%)
Mid-Burnup 2% SEU fuel	0.9	1.6	0.9	2.6
Fresh 2% SEU fuel	0.8	2.1	0.8	2.8
Fresh Graded SEU fuel	0.9	1.6	0.9	3.0

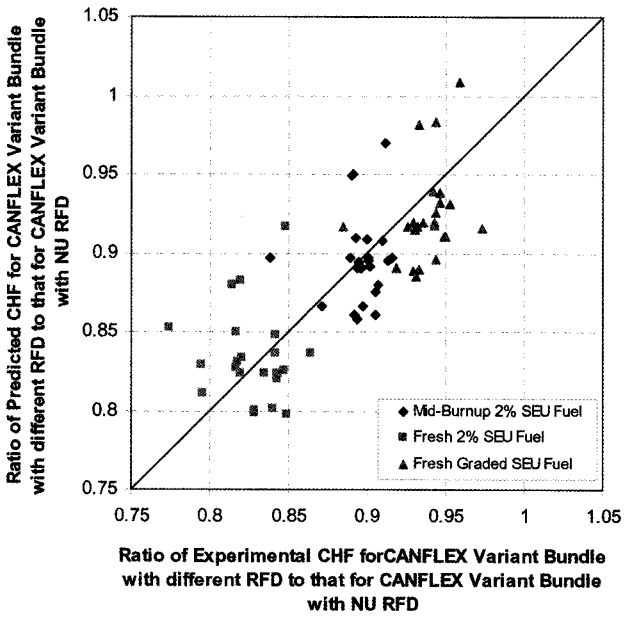

Fig. 10. Comparison of Predicted and Experimental CHF Ratios for Different Radial Power Profiles

the scatter among these ratios are slightly larger for ASSERT-PV predictions than for experimental values. This is probably due to the optimization uncertainty in the correlation representing the ASSERT-PV CHF values for the NU fuel profile.

5. CONCLUSIONS

An assessment of the prediction capability of the ASSERT-PV code on dryout power and CHF has been performed against experimental values obtained with electrically heated, Refrigerant-134a-cooled, bundle simulators in a test loop at CRL. The result shows that

- Dryout power increases with decreasing inlet fluid temperature and increasing mass flow rate, as expected. Measurements agree reasonably well with ASSERT-PV predictions with an average error of ±3%, and a standard deviation of ±5% for various radial power profiles. Dryout power measurements are predicted closely using the ASSERT-PV code, particularly at low flows and low pressures, but are overpredicted at high flows and high pressures. Moreover, the majority of data shows that dryout powers are underpredicted at low inlet-fluid temperatures but overpredicted at high inlet-fluid temperatures.
- CHF increases with decreasing dryout quality, decreasing pressure and increasing mass flux, as expected. Experimental CHF values are overpredicted using ASSERT-PV at high dryout qualities and at high pressure, but underpredicted at low dryout qualities. Differences between experimental values and predictions are probably attributed to the applied modelling options, which were validated for CANFLEX bundle.
- ASSERT-PV predictions follow the same trend, but with different slopes, of CHF values for various radial power profiles. Average predicted CHF ratios between SEU and NU fuel profiles using the ASSERT-PV code agree closely with average experimental ratios. Therefore, the ASSERT-PV code is capable of capturing the relative effect of radial power profile on CHF in the bundle of interest.

REFERENCES

[1] M.B. Carver, J.C. Kiteley, A. Tahir, A.O. Banas, and D.S. Rowe, "Simulation of flow and phase distribution in vertical and horizontal bundles using the ASSERT subchannel code," *Nuclear Engineering and Design*, **122**, pp. 413-424, 1990.

[2] Y.F. Rao and N. Hammouda, "Recent Development in ASSERT-PV Code for Subchannel Thermalhydraulics," *Proceeding of the 8th CNS Int. Conf. on CANDU Fuel*, Sep 21-24, Honey Harbor, Ontario, 2003.

[3] Y. F. Rao and L.K.H. Leung, "Thermalhydraulics Performance Optimization of CANDU Fuel Using ASSERT Subchannel Code," *Proceeding of the 2007 International Congress on Advances in Nuclear Power Plants*, May 13-18, Nice Acropolis, France, 2007.

[4] L.K.H Leung. and D.C. Groeneveld, "Fluid-to-Fluid Modelling of Critical Heat Flux in 37-Element bundles," *Proceedings of the 21st Nuclear Simulation Symposium*, Sept. 24-26, Ottawa, Ontario, 2000.

[5] L.N. Carlucci, N. Hammouda and D.S. Rowe, "Two-Phase Turbulent Mixing and Buoyancy Drift in Rod Bundles," *Nuclear Engineering and Design*, **227**, pp. 65-84, 2004.

[6] G.R. Dimmick, W.W.R. Inch, J.S. Jun, H.C. Suk, G. Haddaller, R. Fortman, and R. Hayes, "Full-Scale Water CHF Testing of the CANFLEX Bundle," *Proceedings of the 6th Int. Conf. on CANDU Fuel*, Niagara Falls, Ontario, 1999.

[7] D.C. Groeneveld, L.K.H. Leung, P.L. Kirillov, V.P. Bobkov, I.P. Smogalev, V.N. Vinogradov, X.C. Huang and E. Royer, "The 1995 Look-up Table for Critical Heat Flux in Tubes," *Nuclear Engineering and Design*, **163**, pp. 1-23, 1996.